Determination of the magnetic ground states in CeNMSb$_2$ compounds with NM = Cu, Ag, Au

Jaekyung Jang ●, Changhyun Yi ●, and Joo Yull Rhee ●*
Department of Physics, Sungkyunkwan University, Suwon 16419, Republic of Korea

In the present work, we investigated the magnetic ground state of CeNMSb$_2$ [NM (noble metal): Cu, Ag, and Au] compounds using electronic-structure calculations while following a full-potential linearized-augmented-plane-wave method. Due to the lack of mirror symmetry about the ab plane, the two Ce atoms—which are located at crystallographically equivalent sites—in a unit cell should be treated inequivalently, and, as a consequence, a $1 \times 1 \times 2$ supercell must be constructed to accommodate the antiferromagnetic (AFM) configuration. The magnetic configuration of the ground state of AFM CeAuSb$_2$ is that the magnetic moments of the two Ce atoms in a conventional unit cell are aligned ferromagnetically and those of an adjacent cell are aligned oppositely along the easy axis. The ground states, including ferromagnetic CeAgSb$_2$ and AFM CeCuSb$_2$, are understood in terms of the exchange interaction J of neighboring Ce atoms. Our results clearly confirm a recent experimental finding, in which, under an external magnetic field ($\lesssim 3$ T) along the c axis, a spin-density wave (SDW) with a wave vector $(\eta, \eta, \frac{1}{2})$, where $\eta \approx 0.136$, is observed in an AFM CeAuSb$_2$ compound. The Fermi surface (FS) on the ab plane exhibits nesting along the (110) direction. The nesting vector $\mathbf{q} = (\zeta, \zeta, 0)$ $(2\pi/a)$, with $\zeta \sim 0.13$, is very similar to the experimental result aside from $\frac{1}{2}$ along the c axis. We argue that the modulation along the c axis is attributed to the period doubling along the c axis due to the lack of mirror symmetry. Although our calculated generalized susceptibility $\chi(\mathbf{q})$ exhibits a pair of peaks along the (110) direction at $\zeta \sim 0.06$ and 0.13, which are related to FS nesting, the peak at $\zeta \sim 0.06$ can hardly be observed in the experiment because of the negligible oscillator strengths of interband transitions at a low $\mathbf{q}$ value. This implies that the observed SDW can be attributed to strong Fermi-surface nesting.

I. INTRODUCTION

The available knowledge on the ground state of quantum materials guides the understanding of a variety of phenomena in condensed-matter physics. For example, it is very important to investigate the ground state of heavy-fermion systems—wherein the effective mass of electrons is often hundreds or even thousands times larger than that of the bare electrons—to elucidate various quantum phenomena, such as non-Fermi-liquid behavior, quantum phase transition, quantum-critical points, etc. [1–6].

CeNMSb$_2$ [NM (noble metal): Cu, Ag, and Au] compounds belong to a family of Ce-based heavy-fermion compounds that exhibit interesting phenomena, such as Kondo-lattice, non-Fermi-liquid, and quantum-critical behaviors under the influence of various nonthermal fluctuations, such as pressure, the external magnetic field, and so on [7–17]. It crystalizes in a ZrCuSi$_2$-type tetragonal structure (space group $P4/nmm$). CeCuSb$_2$ exhibits antiferromagnetic (AFM) ordering along the [100] direction below $T_N \sim 6.9$ K, Kondo-lattice behavior, and small magnetic and strong electrical anisotropy [9,10,18]. CeAgSb$_2$ is a ferromagnet with an easy axis along the [001] direction below ~ 9 K, and it also has strong magnetic anisotropy, anomalous magnetic behavior, and a field-tuned quantum-critical point [10,13,14,19]. CeAuSb$_2$ also exhibits AFM ordering along

the [001] direction below $T_N \sim 6.3$ K, strong magnetic and electrical anisotropy, pressure-induced phase transition, and a temperature- or magnetic-field-tuned quantum-critical point [10,15–17,20].

When working with these compounds, it is necessary to include both the spin-orbit coupling (SOC) and the so-called local density approximation (LDA) $+ U$ method in spin-polarized calculations to predict the correct magnetic easy axis [18,21,22]. It has also been shown that the effects of SOC of Ce $4f$ electrons play a crucial role in determining the magnetic easy axes of these compounds. In particular, it is necessary to treat the two Ce atoms in a unit cell of CeAgSb$_2$ inequivalently—even though the compound is ferromagnetic (FM) and not AFM—because of the lack of mirror symmetry about the ab plane. It should be noted here that the noble metals do not play a significant role in determining the magnetic easy axes. Intuitively, it is tempting to explain that the differences in the magnetic easy axes among the three compounds originate from different noble metals because they are isoelectronic and because their different strengths of SOC seem to be the only source of difference. However, our prior research has shown that the differences in SOC of noble metals play an insignificant role; instead, SOC of Ce plays a fundamental role [21].

It was recently reported that a single-$\mathbf{q}$ spin-density wave (SDW), whose wave vector is $\mathbf{q} = (\eta, \eta, \frac{1}{2})$, with $\eta \cong 0.136$, was maintained up to $\mu_0 H_1 = 2.78$ T and that above H_1 the single-$\mathbf{q}$ SDW was replaced by a coupled harmonic at $\mathbf{q_1} + \mathbf{q_2} = (2\eta, 0, 0) + \mathbf{c}^*$ until $\mu_0 H_2 = 5.42$ T in AFM CeAuSb$_2$

*rheejy@skku.edu

[23]. There was an attempt to explain the physical origin of this incommensurate SDW as the Fermi-surface nesting (FSN), but it was not successful. Independently, Yumnam *et al.* [24] carried out a similar investigation and observed a similar SDW. They also calculated the Fermi surface and found that some nesting surfaces were separated by the experimentally obtained propagation vector.

We examine the ground state of Ce*NM*Sb$_2$ compounds using the electronic-structure calculations with a full-potential linearized-augmented-plane-wave (FPLAPW) method. Because of the lack of mirror symmetry about the *ab* plane, it would be necessary to construct a $1 \times 1 \times 2$ supercell and a $2 \times 2 \times 1$ supercell for the AFM CeAuSb$_2$ and CeCuSb$_2$ compounds, respectively. These results, including the findings regarding FM CeAgSb$_2$, are understood by the spin-exchange interaction J between neighboring Ce atoms. Our results clearly explain the experimental finding in which the wave vector of the SDW is $(\eta, \eta, \frac{1}{2})$, with $\eta \approx 0.136$, for the AFM CeAuSb$_2$ compound. The Fermi surface perpendicular to the *ab* plane exhibits strong nesting along the (110) direction with the nesting vector $\mathbf{q} = (\zeta, \zeta, 0)$ $(2\pi/a)$, with $\zeta \sim 0.13$, which is very close to the results obtained experimentally. The z component, $q_z = \frac{1}{2}$, should not be considered as a real modulation because it is commensurate and can be attributed to the period doubling, which originates from the lack of mirror symmetry about the *ab* plane. To confirm the relation between this FSN and SDW, we calculated the generalized susceptibility $\chi(\mathbf{q})$. As a result, we found that a pair of peaks along the (110) direction at $\zeta \sim 0.05$ and 0.13 are related to FSN. The peak at $\zeta \sim 0.05$ is difficult to see because of negligible interband oscillator strengths in the region of low $\mathbf{q}$.

II. CALCULATIONAL DETAILS

We used the WIEN2K package [25] implemented with the FPLAPW method. The generalized-gradient approximation (GGA) of Perdew, Burke, and Ernzerhof [26] was chosen as the exchange-correlation functional. The muffin-tin radii were 2.5 a.u. for all atoms. We used $RK_{max} = 7$, resulting in ~92 augmented plane waves for the basis functions. For self-consistent-field cycle and Fermi surface plots, we respectively generated 3000 and 50 000 **k** points in the whole Brillouin zone (BZ), which respectively correspond to 724 and 12127 **k** points in an irreducible wedge of BZ. To calculate the generalized susceptibility, the whole reciprocal unit cell was divided into $88 \times 88 \times 18$ parallelepipeds, where each parallelepiped was further cut into six tetrahedra. The **k**-space integration was done using the linear-energy-tetrahedron method [27]. We also included the orbital-dependent potentials, i.e., the so-called LDA $+ U$ method [28] and SOC. When including the LDA $+ U$ method for the Ce 4f orbital, we set the on-site Coulomb interaction to be $U \sim 6.5$ eV and the exchange parameter $J = 0$ for the effective potential $U_{eff} = U - J$. For volume optimization the c/a ratio (for the tetragonal structure) was kept constant and also the atomic positions. The total energies of various unit-cell volumes were calculated and then fitted with the equation of state outlined by Birch-Murnaghan [29]. The experimental lattice constants were taken from Refs. [7,19,30].

III. RESULTS AND DISCUSSION

Ce*NM*Sb$_2$ compounds do not exhibit mirror symmetry about the *ab* plane. Our previous results [21] indicate that this means that the two Ce atoms in the conventional unit cell are inequivalent, once the magnetic easy axis is determined to be along the *c* axis, and that this remains the case even if a compound is ferromagnetic [22]. According to our calculational results, the two Ce atoms in a conventional unit cell of the CeAgSb$_2$ compound have different orbital occupations. For the Ce1 atom only $m = -3$ and $m = 1$ orbitals are occupied, while $m = \pm 3$ and $m = \pm 1$ orbitals are occupied for the Ce2 atom. This different 4f-orbital character of the two Ce atoms in a conventional unit cell clearly manifests the different local electronic environment and the validity of treating the two Ce atoms inequivalently. Therefore, the $1 \times 1 \times 2$ supercell is necessary to accommodate the AFM configuration of the whole crystal. The total magnetic moment is dominated by the Ce atoms, and *NM* and Sb atoms contribute negligibly, as expected. Furthermore, the SOC of Ce 4f electrons plays a crucial role in determining the magnetic easy axes of these compounds and that of *NM* atoms does not play a significant role [21]. Therefore, we can safely conclude that the magnetic structure is mostly determined by Ce atoms. As discussed in detail in the Supplemental Material [31], for the $1 \times 1 \times 2$ supercell construction there are four different AFM configurations that can be used: UDUD ($\uparrow\downarrow\uparrow\downarrow$), DUDU ($\downarrow\uparrow\downarrow\uparrow$), UDDU ($\uparrow\downarrow\downarrow\uparrow$), and UUDD ($\uparrow\uparrow\downarrow\downarrow$) (Fig. S1). Two of these have an AFM configuration in the conventional unit cell and do not require the magnetic unit cell to be doubled along the *c* axis. By contrast, the other two have ferromagnetically coupled bilayers of Ce, and these bilayers are antiferromagnetically coupled with adjacent Ce bilayers. The sequence of spins for Ce atoms is displayed in Fig. 1(a). It should be noted here that those four configurations are all physically distinct from each other because of the lack of mirror symmetry about the *ab* plane. To identify the correct magnetic configuration we performed volume optimizations using the conventional unit cell $(1 \times 1 \times 1)$ and a $1 \times 1 \times 2$ supercell with four different magnetic configurations. Figure 1(b) shows that the total energy per formula unit for the first two configurations in a $1 \times 1 \times 2$ supercell is lower than the corresponding value for a $1 \times 1 \times 1$ unit cell, although period doubling is not required to accommodate the AFM configuration, because a conventional unit cell is already in the AFM configuration. The DUDU and UDUD configurations are almost indistinguishable from each other. As shown in Fig. 1(c), the total energy of UUDD ($\uparrow\uparrow\downarrow\downarrow$) is the lowest, which means that in the ground state the two Ce atoms in a conventional unit cell are coupled ferromagnetically. These results are consistent with those that have been obtained experimentally, which show the presence of $\mathbf{Q} = 2\mathbf{q_1} - \mathbf{c}^*$, which requires that the two Ce^{3+} sites within a unit cell contribute in phase [23]. For AFM CeCuSb$_2$, the total energy of the $1 \times 1 \times 1$ unit cell is lower than that of the $1 \times 1 \times 2$ supercell. However, for AFM CeCuSb$_2$, the construction of the supercell should be considered along the *ab* plane because the direction of the magnetization is not along the *c* axis, but along the in-plane direction. According to our results, the total energy of the $2 \times 2 \times 1$ supercell is lower than that of the $1 \times 1 \times 1$ unit cell and the $1 \times 1 \times 2$ supercell. However, in the case of the $2 \times 2 \times 1$
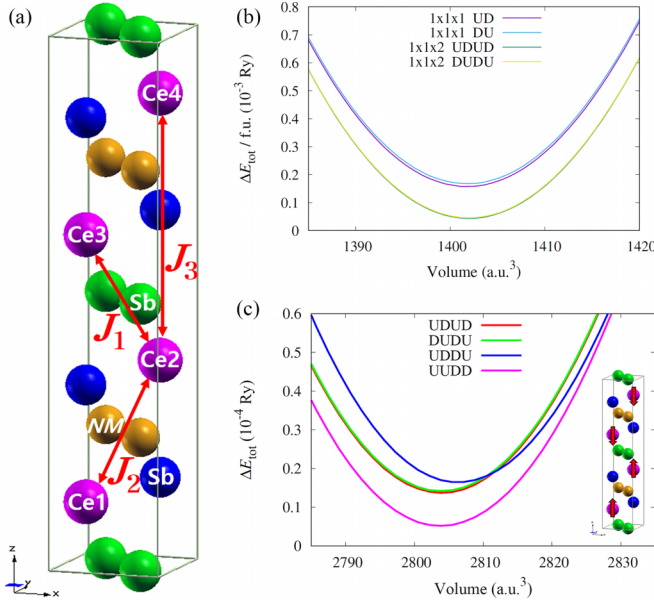
FIG. 1. (a) Crystal structure of CeNMSb$_2$. (b) Volume optimization of two different spin arrangements in the conventional unit cell and corresponding arrangements for a simple period-doubled $1 \times 1 \times 2$ supercell of AFM CeAuSb$_2$. (c) Volume optimization of four different AFM spin configurations for the $1 \times 1 \times 2$ supercell. Here, the total-energy differences relative to a certain value are plotted. The inset of panel (c) shows the "UUDD" or ↑↑↓↓ spin configuration.

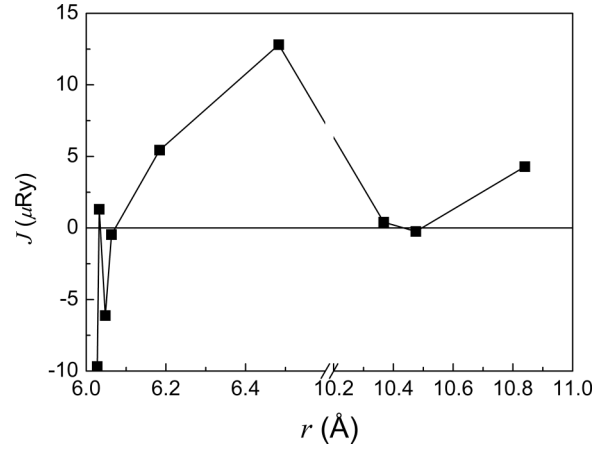FIG. 2. Exchange interaction J as a function of Ce-Ce interatomic distance r, with the solid line as a guide to the eye only.

supercell, there are more magnetic configurations to consider, so the correct magnetic ground state requires additional calculations for AFM CeCuSb$_2$, which are absent here.

To more deeply understand the different ground states of CeNMSb$_2$ compounds, we consider the spin-exchange interaction. Based on the Heisenberg-like model, the spin Hamiltonian can be represented as

$$\mathcal{H} = -\sum_{ij} J_{ij} \mathbf{S}_i \cdot \mathbf{S}_j, \tag{1}$$

where J is the spin-exchange interaction. Here $\mathbf{S}_i \cdot \mathbf{S}_j$ is the total spin of the Ce atoms, having only two values, $+1$ or -1. There are three different exchange terms between Ce atoms, as shown in Fig. 1(a); we denote them as J_1, J_2, and J_3. Here, we did not consider the exchange interactions between the nearest-neighbor and next-nearest-neighbor Ce atoms, which are in the same ab plane as the central Ce atom, because they contribute equally to all magnetic configurations and, therefore, the total-energy differences among various spin configurations can be determined without including these interactions. In calculating the J values, we followed procedures similar to those described in Refs. [32,33]. In comparing total energy, we consider the ground state to be determined by the spin-exchange interaction J and the spin configuration. Figure 2 shows the spin-exchange interaction J as a function of the interatomic distance between neighboring Ce atoms. Here, a positive (negative) sign of J reflects the FM (AFM) configuration. The signs of the J values are consistent with the spin configuration of the ground state, and they exhibit oscillating behavior as the interatomic distance increases. It is

clear that this variation of signs with respect to the interatomic distance between Ce atoms is responsible for the different spin configurations, although it does not explain the different magnetic anisotropy.

To investigate the SDW of AFM CeAuSb$_2$, we plotted FS for the $1 \times 1 \times 2$ supercell. Figure 3 shows the Fermi surfaces on the ab plane with different k_z values. The nesting, which is denoted by a red arrow, is quite robust along the z direction, $\mathbf{q} = (\zeta, \zeta, 0)$ $(2\pi/a)$, and ζ is about 0.13; taken together, these results are very similar to the experimental one obtained for $\eta \approx 0.136$. Yumnam *et al.* [24] also calculated the electronic structures and plotted the Fermi surface, and consequently found a nesting vector very close to the experimental value. There are several important points to note here. First,
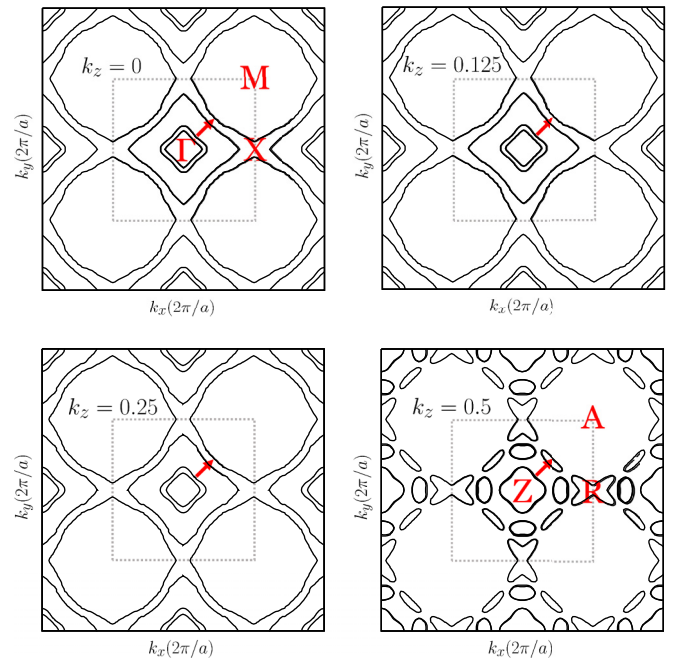

FIG. 3. Fermi surfaces of $1 \times 1 \times 2$ AFM CeAuSb$_2$ along the z direction. Dashed line denotes the first BZ. The nesting vector is denoted by the red arrow, $\mathbf{q} = (\zeta, \zeta, \frac{1}{2})(2\pi/a)$, and ζ is about 0.134.

in their calculation, a $1 \times 1 \times 2$ supercell was used to accommodate various spin configurations. However, their study provided no explicit reasoning for the period doubling along the c axis, and more importantly, there was no discussion of different spin configurations. Although the authors of that study argued that the nesting occurred between two majority-band Fermi surfaces, there should be no difference between the majority bands and the minority bands because CeAuSb$_2$ is in the AFM configuration. Further, the spin-resolved density of states (DOS) shows that the compound is in the FM configuration, not the AFM configuration, because the majority-spin DOS is completely different from the minority-spin DOS. We suspect that the calculations in that study were done for the FM spin configuration. Finally, the Ce $4f$ bands were located at the Fermi level despite the use of the so-called GGA + U method.

Moreover, in the experiment described above, there is a z component of $\mathbf{q}$, $(\frac{1}{2})\mathbf{c}^*$. We speculate that this z component of $\mathbf{q}$ is not due to the modulation that originates from FSN. Although Yumnam *et al.* [24] claimed that their calculations showed almost exactly matching nesting vectors because they found two parallel sheets of FS along the c axis, there is no reason to pick up a particular value of $\frac{1}{2}$ for the z component of $\mathbf{q}$. Instead, we argue that the obtained value of $\frac{1}{2}$ for the z component of $\mathbf{q}$ is attributable to the period doubling along the c axis owing to the lack of mirror symmetry about the ab plane. To check that the z component of the propagation wave vector is due to the period doubling, we plotted and compared the FS of the $1 \times 1 \times 1$ unit cell and the $1 \times 1 \times 2$ supercell (see Ref. [31], Fig. S3). As shown in Fig. S3, the nesting effect, which was not seen clearly at $k_z = 0$ of the $1 \times 1 \times 1$ unit cell, is more clearly visible at $k_z = 0$ of the $1 \times 1 \times 2$ supercell. Since we doubled the unit cell in the z direction, we would expect the FS at $k_z = 0$ of the $1 \times 1 \times 2$ supercell to be equal to the overlap of those at $k_z = 0$ and $k_z = 0.5$ of the $1 \times 1 \times 1$ unit cell. However, in this case, one cannot ignore the effects of band overlap and accidental degeneracies due to unit cell doubling [34]. Consequently, our results show that these effects act to make the FSN more robust at ζ in the case of the $1 \times 1 \times 2$ supercell (see Ref. [31], Fig. S5).

It is generally believed that the existence of density waves in solids, both charge- and spin-density waves, is closely related to the existence of parallel sheets of Fermi surfaces [35]. Therefore, to confirm the relation between FSN and SDW for our results, we calculated the generalized susceptibility $\chi(\mathbf{q})$ [27] of AFM CeAuSb$_2$. The following is used to calculate $\chi(\mathbf{q})$,

$$\chi(\mathbf{q}) = \sum_{n,m,\mathbf{k}} \frac{f[\epsilon_m(\mathbf{k})]\{1 - f[\epsilon_n(\mathbf{k+q})]\}}{\epsilon_n(\mathbf{k+q}) - \epsilon_m(\mathbf{k})} \mathbf{M}_{n\mathbf{k},n'\mathbf{k'}}(\mathbf{q}), \quad (2)$$

where $f(\epsilon)$ is the Fermi-Dirac distribution function, $\epsilon_m(\mathbf{k})$ is the mth band energy at $\mathbf{k}$, and $\mathbf{M}$ is the oscillator-strength matrix elements (MEs). The result of $\chi(\mathbf{q})$ for $\mathbf{q}$ along the (110) direction is shown in Fig. 4. Within the resolution of our calculation, it exhibits two peaks at $\zeta \sim 0.06$ and 0.13. The peak at 0.13 is very well matched with the experiment results. The existence of parallel sheets of Fermi surfaces by nesting results in a large peak in $\chi(\mathbf{q})$ if MEs are assumed to be constant. When nesting features are important, a common
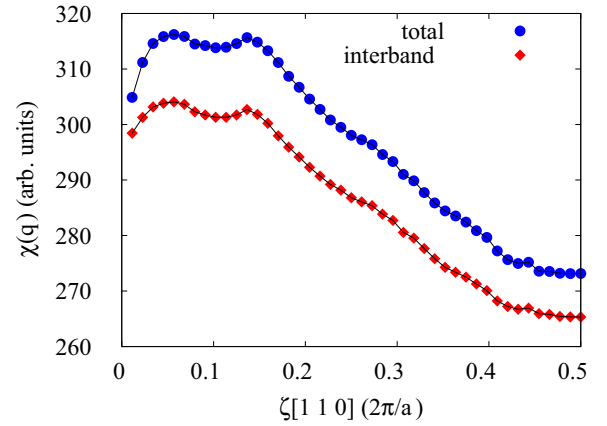

FIG. 4. Generalized susceptibility of AFM CeAuSb$_2$. The solid lines are only meant to serve as visual guides.

method is to regard the MEs,

$$\mathbf{M}_{n\mathbf{k},n'\mathbf{k'}}(\mathbf{q}) = \langle n, \mathbf{k}|e^{-i\mathbf{q}\cdot\mathbf{r}}|n', \mathbf{k'}\rangle, \quad (3)$$

as constant [36–39]. When $\mathbf{q}$ is large the interband matrix elements are dominant, whereas the intraband matrix elements are small. However, in the $\mathbf{q} \rightarrow 0$ limit, the intraband matrix elements almost exhibit unity, while the interband matrix elements vanish. For this reason, in an experiment, it may be difficult to observe the peak at $\mathbf{q} \approx 0.06$ because the contributions from interband transitions are dominant for the whole range of $\mathbf{q}$, as shown in Fig. 4. As shown in Fig. S5 [31], in the case of the $1 \times 1 \times 1$ unit cell, the peak at 0.13 is much weaker than that at 0.06; meanwhile, in the case of the $1 \times 1 \times 2$ supercell, the peak at 0.13, which is very close to the experimental result, is significantly enhanced compared to the case of the $1 \times 1 \times 1$ unit cell. Therefore, we can argue that the finding of $q_z = \frac{1}{2}$ for the SDW wave vector can be attributed to period doubling owing to the lack of mirror symmetry about the ab plane.

IV. CONCLUSION

In summary, we performed electronic-structure calculations for Ce*NM*Sb$_2$ compounds to elucidate the magnetic ground state. Volume-optimization calculations show that the ground state is in the $1 \times 1 \times 2$ supercell construction with the ↑↑↓↓ spin configuration for AFM CeAuSb$_2$ and in the $2 \times 2 \times 1$ supercell for AFM CeCuSb$_2$ along the magnetic easy axes. These different ground states are attributed to differences in the spin-exchange interaction J and the distance of neighboring Ce atoms. The experimental SDW vector $\mathbf{q}$ of AFM CeAuSb$_2$ is well matched with our FS nesting vector $\zeta \sim 0.13$ along the in-plane direction. Although there is a z component in the SDW wave vector, $q_z = \frac{1}{2}$, in the experiment, we argue that this can be attributed to the period doubling stemming from the lack of mirror symmetry. Within the resolution of our calculated generalized susceptibility, we can see a pair of peaks along the (110) direction at $\zeta \sim 0.06$ and 0.13; the peak at $\zeta \sim 0.06$ can hardly be observed in the experiment because of negligible interband oscillator strengths.

ACKNOWLEDGMENTS

[1] G. R. Stewart, Heavy-fermion systems, Rev. Mod. Phys. **56**, 755 (1984).

[2] G. R. Stewart, Non-Fermi-liquid behavior in d- and f-electron metals, Rev. Mod. Phys. **73**, 797 (2001).

[3] H. V. Löhneysen, A. Rosch, M. Vojta, and P. Wölfle, Fermi-liquid instabilities at magnetic quantum phase transitions, Rev. Mod. Phys. **79**, 1015 (2007).

[4] A. Schröder, G. Aeppli, R. Coldea, M. Adams, O. Stockert, H. V. Löhneysen, E. Bucher, R. Ramazashvili, and P. Coleman, Onset of antiferromagnetism in heavy-fermion metals, Nature (London) **407**, 351 (2000).

[5] P. Coleman, C. Pépin, Q. Si, and R. Ramazashvili, How do Fermi liquids get heavy and die? J. Phys.: Condens. Matter **13**, R723 (2001).

[6] P. Gegenwart, Q. Si, and F. Steglich, Quantum criticality in heavy-fermion metals, Nat. Phys. **4**, 186 (2008).

[7] R. V. Skolozdra, J. F. Mikhalski, K. Kaczmarska, and J. Pierre, CeCuSb$_2$ and CeNiSb: new exotic kondo systems, J. Alloys Compd. **206**, 141 (1994).

[8] M. Houshiar, D. T. Adroja, and B. D. Rainford, Kondo lattice behaviour in CeTSb$_2$ compounds (T = Ni, Cu and Ag), J. Magn. Magn. Mater. **140-144**, 1231 (1995).

[9] Y. Muro, N. Takeda, and M. Ishikawa, Magnetic and transport properties of dense Kondo systems, CeTSb$_2$ (T = Ni, Cu, Pd and Ag), J. Alloys Compd. **257**, 23 (1997).

[10] A. Thamizhavel, T. Takeuchi, T. Okubo, M. Yamada, R. Asai, S. Kirita, A. Galatanu, E. Yamamoto, T. Ebihara, Y. Inada, R. Settai, and Y. Ōnuki, Anisotropic electrical and magnetic properties of CeTSb$_2$ (T = Cu, Au, and Ni) single crystals, Phys. Rev. B **68**, 054427 (2003).

[11] T. Koyama, M. Matsumoto, S. Wada, Y. Muro, and M. Ishikawa, Combination of dense Kondo effect and RKKY interactionin CeCuSb$_2$, investigated by NMR, J. Phys. Soc. Jpn. **70**, 3667 (2001).

[12] V. A. Sidorov, E. D. Bauer, N. A. Frederick, J. R. Jeffries, S. Nakatsuji, N. O. Moreno, J. D. Thompson, M. B. Maple, and Z. Fisk, Magnetic phase diagram of the ferromagnetic Kondo-lattice compound CeAgSb$_2$ up to 80 kbar, Phys. Rev. B **67**, 224419 (2003).

[13] P. Logg, Z. Feng, T. Ebihara, Y. Zou, S. Friedemann, P. Alireza, S. Goh, and F. M. Grosche, Pressure and field tuning in the Kondo lattice ferromagnet CeAgSb$_2$, Phys. Status Solidi B **250**, 515 (2013).

[14] Y. Zou, P. Logg, M. Barber, Z. Feng, T. Ebihara, and F. M. Grosche, Thermodynamics of field-tuned quantum critical point in CeAgSb$_2$, Phys. Status Solidi B **250**, 529 (2013).

[15] L. Balicas, S. Nakatsuji, H. Lee, P. Schlottmann, T. P. Murphy, and Z. Fisk, Magnetic field-tuned quantum critical point in CeAuSb$_2$, Phys. Rev. B **72**, 064422 (2005).

[16] S. Seo, V. A. Sidorov, H. Lee, D. Jang, Z. Fisk, J. D. Thompson, and T. Park, Pressure effects on the heavy-fermion antiferromagnet CeAuSb$_2$, Phys. Rev. B **85**, 205145 (2012).

[17] K.-A. Lorenzer, A. M. Strydom, A. Thamizhavel, and S. Paschen, Temperature-field phase diagram of quantum critical CeAuSb$_2$, Phys. Status Solidi B **250**, 464 (2013).

[18] J. Jang and J. Y. Rhee, Peculiar role of f-orbital occupancy in heavy-fermion antiferromagnetic CeNMSb$_2$ (NM: Cu and Au) compounds, Curr. Appl. Phys. **16**, 475 (2016).

[19] S. Araki, N. Metoki, A. Galatanu, E. Yamamoto, A. Thamizhavel, and Y. Ōnuki, Crystal structure, magnetic ordering, and magnetic excitation in the 4f-localized ferromagnet CeAgSb$_2$, Phys. Rev. B **68**, 024408 (2003).

[20] S. Seo, X. Wang, S. M. Thomas, M. C. Rahn, D. Carmo, F. Ronning, E. D. Bauer, R. D. dos Reis, M. Janoschek, J. D. Thompson, R. M. Fernandes, and P. F. S. Rosa, Nematic State in CeAuSb$_2$, Phys. Rev. X **10**, 011035 (2020).

[21] J. Jang, M. M. Alsardia, and J. Y. Rhee, Magnetic ground state of ferromagnetic CeAgSb$_2$, J. Magn. Magn. Mater. **477**, 283 (2019).

[22] M. M. Alsardia, J. Jang, and J. Y. Rhee, Pressure effects on the magnetic phase diagram of the CeNMSb$_2$ (NM: Au and Ag): A DFT study, Materials **13**, 2237 (2020).

[23] G. G. Marcus, D.-J. Kim, J. A. Tutmaher, J. A. Rodriguez-Rivera, J. O. Birk, C. Niedermeyer, H. Lee, Z. Fisk, and C. L. Broholm, Multi-q mesoscale magnetism in CeAuSb$_2$, Phys. Rev. Lett. **120**, 097201 (2018).

[24] G. Yumnam, Y. Chen, Y. Zhao, A. Thamizhavel, S. K. Dhar, and D. K. Singh, Microscopic nature of magnetic ground state in CeAuSb$_2$, Phys. Status Solidi RRL **13**, 1900304 (2019).

[25] P. Blaha, K. Schwarz, G. K. H. Madsen, D. Kvasnicka, J. Luitz, R. Laskowski, F. Tran, and L. D. Marks, *Wien2k: An Augmented Plane Wave + Local Orbitals Program for Calculating Crystal Properties* (Vienna University of Technology, Austria, 2018).

[26] J. P. Perdew, K. Burke, and M. Ernzerhof, Generalized gradient approximation made simple, Phys. Rev. Lett. **77**, 3865 (1996).

[27] J. Rath and A. J. Freeman, Generalized magnetic susceptibilities in metals: Application of the analytic tetrahedron linear energy method to Sc, Phys. Rev. B **11**, 2109 (1975).

[28] V. I. Anisimov, I. V. Solovyev, M. A. Korotin, M. T. Czyżyk, and G. A. Sawatzky, Density-functional theory and NiO photoemission spectra, Phys. Rev. B **48**, 16929 (1993).

[29] F. Birch, Finite elastic strain of cubic crystals, Phys. Rev. **71**, 809 (1947).

[30] O. Sologub, K. Hiebl, P. Rogl, H. Noël, and O. Bodak, On the crystal structure and magnetic properties of the ternary rare earth compounds RETSb$_2$ with RE ≡ rare earth and T ≡ Ni, Pd, Cu and Au, J. Alloys Compd. **210**, 153 (1994).

[31] See Supplemental Material at http://link.aps.org/supplemental/10.1103/PhysRevB.109.054431 for antiferromagnetic configurations, Fermi surfaces, and generalized susceptibility.

[32] D. Ködderitzsch, W. Hergert, W. M. Temmerman, Z. Szotek, A. Ernst, and H. Winter, Exchange interactions in NiO and at the NiO(100) surface, Phys. Rev. B **66**, 064434 (2002).

[33] X. Rocquefelte, M.-H. Whangbo, A. Villesuzanne, S. Jobic, F. Tran, K. Schwarz, and P. Blaha, Short-range magnetic order

and temperature-dependent properties of cupric oxide, J. Phys.: Condens. Matter **22**, 045502 (2010).

[34] C. Herring, Accidental degeneracy in the energy bands of crystals, Phys. Rev. **52**, 365 (1937).

[35] G. Grüner, *Density Waves in Solids* (Perseus, Cambridge, MA, 1994).

[36] A. J. Freeman, T. J. Watson-Yang, and J. Rath, Generalized susceptibilities and phonon anomalies in Pd and Pt metals, J. Magn. Magn. Mater. **12**, 140 (1979).

[37] H. W. Myron, J. Rath, and A. J. Freeman, Generalized electronic susceptibility and charge-density waves in $1T - TaS_2$ and $1T - TaSe_2$, Phys. Rev. B **15**, 885 (1977).

[38] M. Gupta, A. J. Freeman, and D. E. Ellis, Electronic structure and lattice instability of metallic VO_2, Phys. Rev. B **16**, 3338 (1977).

[39] M. Posternak, A. J. Freeman, and D. E. Ellis, Electronic band structure, optical properties, and generalized susceptibility of NbO_2, Phys. Rev. B **19**, 6555 (1979).